

Fluid dynamics and noise in bacterial cell–cell and cell–surface scattering

Knut Drescher^a, Jörn Dunkel^a, Luis H. Cisneros^b, Sujoy Ganguly^a, and Raymond E. Goldstein^{a,1}

^aDepartment of Applied Mathematics and Theoretical Physics, University of Cambridge, Wilberforce Road, Cambridge CB3 0WA, United Kingdom; and ^bDepartment of Physics, University of Arizona, 1118 East 4th Street, Tucson, AZ 85721

Edited* by Jerry P. Gollub, Haverford College, Haverford, PA, and approved May 18, 2011 (received for review December 20, 2010)

Bacterial processes ranging from gene expression to motility and biofilm formation are constantly challenged by internal and external noise. While the importance of stochastic fluctuations has been appreciated for chemotaxis, it is currently believed that deterministic long-range fluid dynamical effects govern cell–cell and cell–surface scattering—the elementary events that lead to swarming and collective swimming in active suspensions and to the formation of biofilms. Here, we report direct measurements of the bacterial flow field generated by individual swimming *Escherichia coli* both far from and near to a solid surface. These experiments allowed us to examine the relative importance of fluid dynamics and rotational diffusion for bacteria. For cell–cell interactions it is shown that thermal and intrinsic stochasticity drown the effects of long-range fluid dynamics, implying that physical interactions between bacteria are determined by steric collisions and near-field lubrication forces. This dominance of short-range forces closely links collective motion in bacterial suspensions to self-organization in driven granular systems, assemblages of biofilaments, and animal flocks. For the scattering of bacteria with surfaces, long-range fluid dynamical interactions are also shown to be negligible before collisions; however, once the bacterium swims along the surface within a few microns after an aligning collision, hydrodynamic effects can contribute to the experimentally observed, long residence times. Because these results are based on purely mechanical properties, they apply to a wide range of microorganisms.

low Reynolds number hydrodynamics | microswimmers

Collective behavior of bacteria, such as biofilm formation (1), swarming (2), and turbulence-like motion in concentrated suspensions (3, 4), has profound effects on foraging, signaling, and transport of metabolites (5, 6), and can be of great biomedical importance (7, 8). Large-scale coherence in bacterial systems typically arises from a combination of biochemical signaling (9) and physical interactions. Recent theoretical models that focus on physical aspects of bacterial dynamics identify pairwise long-range hydrodynamic interactions (10–16) as a key ingredient for collective swimming. Such “microscopic” approaches underpin continuum theories that aim to describe the phenomenology of microbial suspensions (17–23). An assumption underlying many of these theories is that a self-propelled bacterium can be modeled as a force dipole; its body exerts a drag force F on the fluid that is balanced by the rearward flagellar thrust $-F$. The leading-order fluid velocity field at distance r is therefore a dipolar “pusher” flow of magnitude $u \propto F\ell/\eta r^2$ (see streamlines in Fig. 1*B*), where η is the viscosity, and ℓ the distance between the forces (24, 25). While higher order corrections may be due to force-quadrupole contributions (26), the hypothesis that the leading-order flow field around a bacterium is dipolar has not yet been verified experimentally.

A closely related, controversially discussed issue (27–30) is the relevance of long-range hydrodynamic interactions in the scattering of bacteria with surfaces, a phenomenon intimately linked with surface accumulation and biofilm formation. Cell–surface scattering is very similar to cell–cell scattering, because, by analogy with image charges in electrostatics, a bacterium that swims

near a surface induces an “image bacterium” on the opposite side of the wall to yield the no-slip boundary condition on the surface (27, 31); bacterium–surface scattering can therefore be analyzed as the interaction of a bacterium with its hydrodynamic image. Several recent calculations for microswimmers near surfaces have found that pusher-type organisms (those with thrust generated behind the cell body) should display a passive stable alignment of the swimming direction with the wall (27, 32–35). However, direct measurements of the three-dimensional swimming tracks of bacteria near surfaces suggest that they simply collide with the surface (28, 36). This raises the question: Is this discrepancy between experiment and theory due to incomplete knowledge of the bacterial flow field, or is the magnitude of the flow so small that fluid-mediated interactions are irrelevant?

The need for experimental tests of the force dipole assumption and, more generally, of the relevance of fluid-mediated interactions for bacteria, is further illustrated by recent measurements on *Chlamydomonas reinhardtii* (37, 38), the archetypal “puller” microorganism (thrust generation in front of the cell body) that was thought to generate a simple force dipole flow with opposite sign to the bacterial one (25). Surprisingly, these experiments showed that while such a dipolar flow exists at large distances from the organism, in regions where the flow magnitudes are significant (greater than 1% of the swimming speed), the flow topology is qualitatively different and more accurately described in terms of a triplet of force singularities (one for the cell body and one for each flagellum) (37). Here we present direct measurements of the flow field around individual freely swimming bacteria, using *Escherichia coli* as a model. We find that the pusher force dipole provides a good approximation to the flow field both when the organism is far from surfaces and close to a no-slip boundary, yet the magnitude of the flow is very low in both cases. Using the experimentally determined flow field parameters, the hydrodynamic interaction of two *E. coli* can be calculated, and it is found to be washed out by rotational diffusion of the swimming direction for closest encounter distances $\gtrsim 3 \mu\text{m}$ —a result that should hold for many other bacterial species due to the similarity of motility parameters. Similarly, analysis of cell–surface encounters suggests that hydrodynamics plays a negligible role, except when a bacterium swims along a surface at a small distance (less than a few microns) after an inelastic aligning collision. In this case, hydrodynamic effects can contribute to the observed long residence times near surfaces.

Results

Flow Field Far from Surfaces. To resolve the miniscule flow field created by bacteria, individual *gfp*-labeled, nontumbling *E. coli*

Author contributions: K.D., J.D., L.H.C., S.G., and R.E.G. designed research; K.D., J.D., and R.E.G. performed research; K.D. and J.D. analyzed data; and K.D., J.D., and R.E.G. wrote the paper.

The authors declare no conflict of interest.

*This Direct Submission article had a prearranged editor.

¹To whom correspondence should be addressed. E-mail: R.E.Goldstein@damtp.cam.ac.uk.

This article contains supporting information online at www.pnas.org/lookup/suppl/doi:10.1073/pnas.1019079108/-DCSupplemental.

were tracked as they swam through a suspension of fluorescent tracer particles (see *Materials and Methods*). Measurements far from walls were obtained by focusing on a plane 50 μm from the top and bottom surfaces of the sample chamber, and recording approximately 2 terabytes of movie data. Within this data we identified approximately 10^4 rare events when cells swam within the depth of field (2 μm thick) for >1.5 s. By tracking the fluid tracers during each of the rare events, relating their position and velocity to the position and orientation of the bacterium, and performing an ensemble average over all bacteria, the time-averaged flow field in the swimming plane was determined down to 0.1% of the mean swimming speed $V_0 = 22 \pm 5$ $\mu\text{m/s}$. As *E. coli* rotate about their swimming direction, their time-averaged flow field in three dimensions is cylindrically symmetric. The present measurements capture all components of this cylindrically symmetric flow except the azimuthal flow due to the rotation of the cell about its body axis. In contrast with the flow around higher organisms such as *Chlamydomonas* (37, 38) and *Volvox* (37), the topology of the measured bacterial flow field (Fig. 1A) is that of a force dipole (shown in Fig. 1B). Yet, there are some differences between the force dipole flow and the measurements close to the cell body, as shown by the residual of the fit (Fig. 1C).

The decay of the flow speed with distance r from the center of the cell body (Fig. 1D) illustrates that the measured flow field displays the characteristic $1/r^2$ form of a force dipole. However, the force dipole model significantly overestimates the flow to the side and behind the cell body, where the measured flow magnitude is nearly constant over the length of the flagellar bundle. The force dipole fit to the far field ($r > 8$ μm) was achieved with two

opposite force monopoles (Stokeslets) at variable locations along the swimming direction. As $r = 0$ corresponds to the center of the cell body in Fig. 1D, and not the halfway point between the two opposite Stokeslets, the fit captures some of the anterior-posterior asymmetry in the flow magnitude u . From the best fit, which is insensitive to the specific algorithms used, we obtained the dipole length $\ell = 1.9$ μm and dipole force $F = 0.42$ pN. This value of F is consistent with optical trap measurements (39) and resistive force theory calculations (40). It is interesting to note that in the best fit, the cell drag Stokeslet is located 0.1 μm behind the center of the cell body, possibly reflecting the fluid drag on the flagellar bundle.

Flow Field Near a Surface. Having found that a force dipole flow describes the measured flow around *E. coli* with good accuracy in the bulk (far from boundaries), we investigated whether this approximation is also valid when *E. coli* swim close to a wall. Focusing 2 μm below the top of the sample chamber, and applying the same measurement technique as before, we obtained the flow field shown in Fig. 1E. This flow decays much faster than that in the bulk due to the proximity of a no-slip surface (Fig. 1H), and the inward and outward streamlines are now joined to produce loops (Fig. 1E). However, both of these differences are consistent with a simple force dipole model and are therefore not due to a change in bacterial behavior. In particular, closed streamlines are known to be a rather general feature of point singularities near no-slip surfaces (41). Using the solution of a Stokeslet near a wall (31) to obtain that of a force dipole near a wall yields streamlines (Fig. 1F) and a decay (Fig. 1H) of the

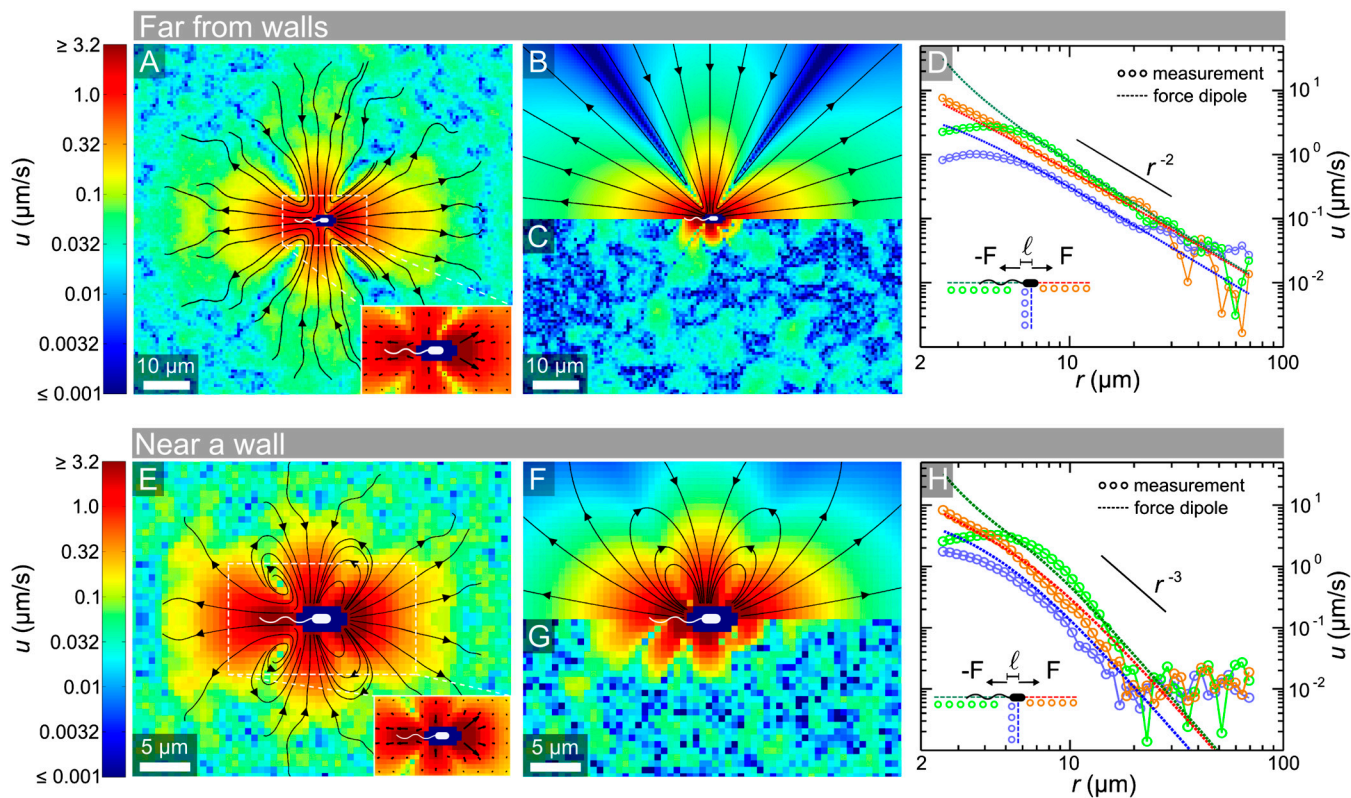


Fig. 1. Average flow field created by a single freely swimming bacterium far from surfaces (A–D) and close to a wall (E–H). Streamlines indicate the local direction of flow, and the logarithmic color scheme indicates flow speed magnitudes. (A) Experimentally measured flow field in the bacterial swimming plane, with the inset showing the anterior-posterior asymmetry close to the cell body. (B) Best-fit force dipole flow. (C) Residual flow field, obtained by subtracting the best-fit dipole model from the measured field. (D) Radial decay of the flow speed u in different directions, with $r = 0$ corresponding to the center of the cell body. For distances $r \lesssim 6$ μm the dipole model overestimates the flow field behind and to the side of the cell body. (E) Experimentally measured flow field in the bacterial swimming plane, for bacteria swimming parallel to a wall at a distance of 2 μm . (F) Best-fit force dipole flow, where the presence of the wall causes inward and outward streamlines to join. (G) Residual flow field. (H) The flow speed decays much faster for bacteria swimming close to a wall, as the fluid velocity must vanish on the surface.

flow field that is consistent with the data. The best-fit force dipole in this geometry yields $F = 0.43$ pN and $\ell = 2.2$ μm , consistent with the values obtained far from walls, but less accurate than those values due to the much faster decay of $u(r)$ near a wall.

Spectral Flow Analysis. To analyze systematically the angular flow structure even at distances $r < 6$ μm , where the force dipole model overestimates the flow magnitudes, it is useful to decompose the flow field into vector spherical harmonics. The resulting spectra are useful “fingerprints” of the flow field that can be compared among many different organisms, and against theoretical models. Such a spectral analysis is described in the *SI Text*.

Rotational Diffusion. Even bacteria that do not display tumbles, such as those studied here, do not swim in completely straight lines. Random changes in swimming direction due to thermal effects and intrinsic noise in the swimming apparatus lead to rotational diffusion, which can be characterized by a coefficient D_r . From the swimming data recorded for *E. coli* far from surfaces, we measured $D_r = 0.057$ rad^2/s (see *Materials and Methods*). Even organisms that are too large to have significant thermal rotational diffusion, such as the 10- μm sized alga *Chlamydomonas reinhardtii*, can have a significant D_r due to noise in the swimming mechanism (42). From swimming data previously recorded for *Chlamydomonas* (37), we found $D_r = 0.4$ rad^2/s .

Discussion

Our measurements show that, independently of whether *E. coli* swim near or far from a surface, their flow field can be described to good accuracy by a simple force dipole model whose parameters we determined. We now proceed to discuss the implications of this flow field for cell–cell and cell–surface interactions. Based on the measured parameters and the force dipole approximation, we calculate the effect of long-range hydrodynamics for these two scattering phenomena and evaluate the importance of fluctuations in the swimming direction.

Hydrodynamics vs. Rotational Diffusion in Cell–Cell Scattering. Fluid-mediated long-range interactions are thought to play an important role in collective motion in bacterial suspensions (17–23). These deterministic interactions, however, compete with rotational diffusion of the swimming direction. To infer the importance of long-range hydrodynamics in the bulk, we consider the change in swimming direction of a bacterium due to hydrodynamic scattering with another bacterium. This can be done by fixing one bacterium at the origin and examining the trajectory of the other. The flow field around the bacterium at the origin is approximated by that of a point force dipole (31)

$$\mathbf{u}(\mathbf{r}) = \frac{A}{|\mathbf{r}|^2} [3(\hat{\mathbf{r}} \cdot \mathbf{d}')^2 - 1] \hat{\mathbf{r}}, \quad A = \frac{\ell F}{8\pi\eta}, \quad \hat{\mathbf{r}} = \frac{\mathbf{r}}{|\mathbf{r}|}, \quad [1]$$

where \mathbf{d}' is the unit vector in the swimming direction, and \mathbf{r} is now the distance vector relative to the center of the dipole. The evolution of the position \mathbf{x} and swimming direction \mathbf{d} of the second swimmer in this field obeys (43)

$$\dot{\mathbf{x}} = V_0 \mathbf{d} + \mathbf{u}, \quad [2]$$

$$\dot{\mathbf{d}} = \frac{1}{2} \boldsymbol{\omega} \times \mathbf{d} + \Gamma \mathbf{d} \cdot \mathbf{E} \cdot (\mathbf{I} - \mathbf{d}\mathbf{d}), \quad [3]$$

where \mathbf{I} is identity matrix, and the central swimmer leads to an advective flow \mathbf{u} , a vorticity $\boldsymbol{\omega}$, and a strain-rate tensor \mathbf{E} at the position \mathbf{x} (see *SI Text* for exact expressions of these quantities). By examining the evolution of $\mathbf{d}(t)$ in a scattering process that begins at $-t/2$, reaches a minimal encounter distance r at $t = 0$, and ends at $t/2$, the mean squared angular change of orientation during a time interval t can be computed as

$$\langle \Delta\phi(t, r)^2 \rangle_H = \langle \arccos[\mathbf{d}(-t/2) \cdot \mathbf{d}(t/2)]^2 \rangle_H, \quad [4]$$

where $\langle \cdot \rangle_H$ indicates an average over all possible orientations and positions of encounters. Assuming that the interaction time scale of the two bacteria τ is small, and using the force dipole model from Eq. 1 we obtain (see derivation in *SI Text*)

$$\langle \Delta\phi(\tau, r)^2 \rangle_H = \frac{3}{5} (\Gamma + 1)^2 \frac{A^2 \tau^2}{r^6}, \quad [5]$$

where $\Gamma \sim 1$ is a geometric factor for *E. coli*. Intuitively, this form arises from the fact that $\Delta\phi \sim \omega\tau$, where the vorticity magnitude ω falls off as A/r^3 . To evaluate the importance of hydrodynamic interactions relative to random fluctuations, we compare $\langle \Delta\phi(\tau, r)^2 \rangle_H$ with the angular diffusion due to Brownian motion and intrinsic swimming variability in three dimensions, given by $\langle \Delta\phi(t)^2 \rangle_D = 4D_r t$. Balancing the effects of hydrodynamics and noise,

$$\langle \Delta\phi(\tau, r_H)^2 \rangle_H = \langle \Delta\phi(\tau)^2 \rangle_D, \quad [6]$$

defines an effective hydrodynamic horizon r_H , beyond which noise dominates over hydrodynamics. For scattering events with closest encounter distances $r > r_H$ hydrodynamics is therefore practically irrelevant. From this definition of r_H and Eq. 5, we find

$$r_H \simeq \left[\frac{3}{20} (\Gamma + 1)^2 \frac{A^2 \tau^2}{D_r} \right]^{1/6}. \quad [7]$$

Due to the $\tau^{1/6}$ -dependence, the hydrodynamic horizon r_H is rather insensitive to the particular value used for the interaction time scale τ and, similarly, to changes in the other parameters. Using the measured values $D_r = 0.057$ rad^2/s , $V_0 = 22$ $\mu\text{m}/\text{s}$, $A = 31.8$ $\mu\text{m}^3/\text{s}$, and adopting $\tau = a/V_0 \simeq 0.1$ s, where $a = 3$ μm is the length of the cell body, we obtain $r_H \simeq 3.3$ μm for *E. coli*. This value of r_H is an upper bound, because the dipolar flow model overestimates \mathbf{u} for $r \lesssim 6$ μm (Fig. 1D). At such small separations, however, steric repulsion, flagellar intertwining, and lubrication forces dominate the physical cell–cell interactions (44, 45). For the mean distance between *E. coli* to reach r_H , the volume fraction needs to be as high as 5–10%. Using our measured parameters in a recent theoretical calculation (46) of the critical volume fraction for the onset of collective swimming due to hydrodynamic interactions leads to an even higher value, implying that a complete analysis of collective behavior in bacterial suspensions must account for steric and near-field interactions.

More generally, we expect similar results to hold for various types of swimming bacteria (e.g., *Pseudomonas aeruginosa*, *Vibrio cholerae*, *Salmonella typhimurium*), as the parameters ($a, \tau, D_r, F\ell$) are similar across many genera. Larger organisms may display even stronger rotational diffusion due to enhanced intrinsic swimming stochasticity (42). For example, the alga *Chlamydomonas* ($a \simeq 10$ μm , $V_0 \simeq 100$ $\mu\text{m}/\text{s}$) has $D_r \simeq 0.4$ rad^2/s . Although the flow topology around *Chlamydomonas* is more complicated than that around bacteria, *Chlamydomonas* still produces a $1/r^2$ field (37), so that our previously calculated result for the bacterial hydrodynamic horizon may be used to give an estimate of $r_H \sim 7.5$ μm , again on the scale of the organism. Thus, collisions, rather than long-range hydrodynamics, can also govern scattering events of higher microorganisms. However, for organisms that produce fast flows, have a long interaction time τ , and a negligible D_r , like the alga *Volvox*, long-range hydrodynamic interactions are significant (47).

Cell–Surface Scattering. The accumulation of bacteria near surfaces is a key step during the initial stages of biofilm formation, and it has been suggested that long-range hydrodynamics plays an important role in bacteria–surface interactions (27). Because

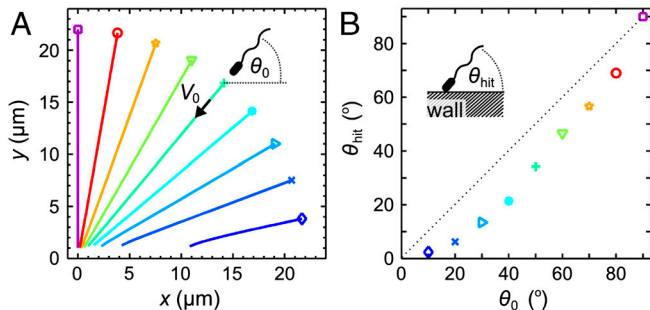


Fig. 2. Simulated dynamics of an *E. coli*-like force dipole swimmer near a wall. (A) Deterministic swimming trajectories towards a wall at $y = 0$, numerically simulated from Eqs. 2 and 3, where \mathbf{u} , $\boldsymbol{\omega}$, and \mathbf{E} are due to the hydrodynamic image system. Simulations used a time step $\Delta t = 10^{-5}$ s and the experimentally determined parameters $A = 31.8 \mu\text{m}^3/\text{s}$, $V_0 = 22 \mu\text{m}/\text{s}$ and $\Gamma = 0.88$ for the force dipole swimmer. The initial distance is chosen such that the swimmer would reach the wall after 1 s if hydrodynamic interactions were not present. (B) Incidence angle θ_0 vs. collision angle θ_{hit} with the wall for the trajectories in A, using the same symbols and colors. The dotted line indicates $\theta_{\text{hit}} = \theta_0$. Both panels illustrate that hydrodynamic long-range interactions can be regarded as small perturbations for typical wall scattering events of *E. coli*.

our measurements show that the flow field has a small amplitude, it is plausible that bacterial cell–surface scattering events could be described instead by nearly straight-line swimming interrupted by collisions with the wall that lead to alignment with the surface due to near-field lubrication and/or steric forces during the collision (28). Our experimental results establish the key microscopic parameters required for a systematic investigation of whether long-range hydrodynamic interactions are relevant to bacteria–surface scattering.

As a first step in our analysis, we performed numerical scattering studies by simulating the deterministic equations of motion for an *E. coli*-like pusher force dipole swimmer in the presence of an infinite no-slip surface. The equations of motion of the swimmer position \mathbf{x} and unit orientation vector \mathbf{d} are simply those used above (Eqs. 2 and 3) except that now \mathbf{u} , $\boldsymbol{\omega}$, and \mathbf{E} are quantities arising from the hydrodynamic image system in the wall (exact expressions for these quantities are given in the *SI Text*). By restricting ourselves to simulations of the deterministic dynamics at this stage, we overestimate the relevance of hydrodynamic long-range interactions between the swimmer and the wall, because rotational diffusion of the swimming direction further diminishes hydrodynamic effects. However, even without rotational diffusion our simulations show that long-range interactions of swimmers with the wall have little effect on the swimming dynamics (Fig. 2). The trajectories of force dipole swimmers that swim toward the wall from different initial angles θ_0 are depicted in Fig. 2A. The initial distance was chosen such that the swimmer would reach the wall plane ($y = 0$) after 1 s if hydrodynamic interactions were absent. Each simulation is stopped when a volume around the swimmer (a bacterial shape of length 3 μm and diameter 0.8 μm) crosses the wall. Fig. 2B displays the impact angle θ_{hit} as a function of the initial angle θ_0 , illustrating that the difference between incidence and collision angles is small unless the swimmer already has a small angle of incidence. These simulations indicate that hydrodynamic long-range interactions are not likely to play an important role in cell–surface scattering for *E. coli*. Because the swimming parameters are similar for many bacterial species, we again expect this result to apply more generally.

Trapping by Surfaces. When *E. coli* swim very close to a surface (approximately 1–3 μm), we observed that individual bacteria spend an average of 64 s (standard error 4 s) next to the wall (within the focal plane). Effective trapping by electrostatic attrac-

tion is unlikely, because both the *E. coli* outer cell wall and the chamber walls (bovine serum albumin coated onto PDMS) (48) are negatively charged in our liquid medium (we observed similarly long residence times on simple glass surfaces). However, the surprisingly long residence times could be caused by the suppression of rotational diffusion due to geometric constraints on the orientation of the cell body and flagella near a surface. Although we showed in the previous section that hydrodynamics has a very small effect on the swimming direction before collisions with the surface, hydrodynamic attraction by the surface (27) could contribute to the observed trapping periods when a bacterium is already very close to the surface. Considering only hydrodynamic attraction counteracted by rotational diffusion, we now derive approximate expressions for the mean escape time t_e and escape height above the surface h_e , by mapping the underlying escape process onto a Kramers problem (49, 50) for the noise-induced escape over a potential barrier. The main arguments and implications are summarized below, while a detailed derivation is given in the *SI Text*.

We again approximate the *E. coli* flow field by the dipole model, because a force dipole placed close to a wall accurately captures the measured flow field parallel to the surface (see Fig. 1 E–H). Thus, Eq. 1 is modified to account for the presence of the wall (31), as discussed in the *SI Text*, and near-field hydrodynamic lubrication effects are neglected. A bacterium is able to escape from the surface, if its swimming velocity component perpendicular to the surface, $V_0 \sin \theta$, exceeds the attraction from its hydrodynamic image (see *SI Text*), which yields the defining relation for the escape angle θ_e ,

$$\sin \theta_e = \Lambda [1 - 3(\sin \theta_e)^2], \quad \Lambda = \frac{3A}{8h^2 V_0}. \quad [8]$$

For *E. coli* swimming at distances $h > 1.5 \mu\text{m}$ from the wall, the escape angles are small, $\theta_e(h) < 11^\circ \ll 1$ rad so that linearization of Eq. 8 is a good approximation, giving $\theta_e \simeq \Lambda$.

After colliding with the wall, a bacterium may have a small positive angle $\theta < \theta_e$ with the surface. The equation of motion for θ can then be rewritten as a Langevin equation (49) in terms of the derivative of an effective “potential” $U(\theta)$, and a diffusion term with Gaussian white noise $\xi(t)$,

$$\dot{\theta} = -\frac{dU}{d\theta} + (2D_r^*)^{1/2} \xi(t), \quad U(\theta) \simeq \frac{\theta^2}{2\kappa}, \quad [9]$$

where the approximation $\theta \ll 1$ reduces $U(\theta)$ to a harmonic potential, yielding a time scale $\kappa = 16h^3/(9A)$ that characterizes hydrodynamic realignment. D_r^* is the rotational diffusion constant close to the surface in the direction perpendicular to the surface, which is expected to be smaller than our measured value $D_r = 0.057 \text{ rad}^2/\text{s}$ far from boundaries, due to geometric constraints on the bacterial orientation near a surface. The generic form of this Langevin equation means that finding the residence time for a bacterium near a wall is a Kramers problem (49, 50) for the escape over a barrier ΔU . Because the organism can escape if $\theta > \theta_e$, we have $\Delta U = U(\theta_e)$.

By considering the height at which $\Delta U = D_r^*$ —i.e., the distance at which the hydrodynamic torque barrier is comparable to the diffusion “temperature”—we can obtain an expression for the escape height

$$h_e = \frac{1}{2} \left(\frac{81 A^3}{16 D_r^* V_0^2} \right)^{1/7}. \quad [10]$$

Using our measured values for *E. coli*, we find $h_e = 1.7 \mu\text{m} \times (D_r/D_r^*)^{1/7}$, illustrating that hydrodynamics is practically negligible if *E. coli* are more than a cell length away from the wall.

As long as the torque exerted by the hydrodynamic image is small ($\Delta U \ll D_r^*$) the typical escape time is set by the rotational diffusion time scale θ_e^2/D_r^* . For high barriers $\Delta U \gg D_r^*$ [in practice, $\Delta U > 3D_r^*$ often suffices, yielding $h \lesssim 1.5 \times (D_r/D_r^*)^{1/7} \mu\text{m}$], transition state theory (49) implies that the mean escape time is modified by an Arrhenius-Kramers factor, so that approximately

$$t_e(h) \approx \left(\frac{\theta_e^2}{D_r^*}\right) \exp\left(\frac{\Delta U}{D_r^*}\right). \quad [11]$$

Using the quadratic approximation for ΔU , and Eq. 10 to express D_r^* in terms of h_e , we find that $t_e \propto \exp(h_e/h)^7$. This dramatic scaling arises from the fact that the dipole model overestimates the flow field close to the bacterium but generally hints at the possibility of a strong, hydrodynamically induced increase of t_e when the cells get closer to the surface. We may also evaluate Eq. 11 at a height $h = 1.5 \mu\text{m}$, where both the Arrhenius-Kramers factor and the approximation $\theta_e(h) \ll 1$ are valid, to give

$$t_e \approx 0.78 \text{ s} \times \left(\frac{D_r}{D_r^*}\right) \exp\left[1.99 \times \left(\frac{D_r}{D_r^*}\right)\right]. \quad [12]$$

The latter estimate suggests that hydrodynamic effects can possibly explain the experimentally observed long residence times near a wall, even for values of D_r/D_r^* that are only moderately larger than 1. It is, however, important to note that this expression for t_e presents an upper bound, because the dipole model overestimates the actual flow field at distances $< 6 \mu\text{m}$ from the bacterium (Fig. 1H), even though the model still correctly captures the flow topology.

The considerations above show that hydrodynamics is negligible if a bacterium is more than a body length away from the wall but that hydrodynamic effects may contribute to the experimentally observed long residence times of bacteria close to no-slip surfaces. A more detailed understanding of the escape problem remains an important future challenge, requiring new methods for measuring D_r^* and further theoretical studies of the near-field interactions between bacteria, their flagella, and surfaces. However, even if a more accurate description of the hydrodynamics should become available in the future, one can still expect the mean escape time to follow an Arrhenius-Kramers law (as in Eq. 11) with a suitably adapted effective potential U and additional prefactors that account for the curvature at the potential barrier (49).

Conclusions

We have presented direct measurements of the flow field generated by individual freely swimming bacteria, both in bulk fluid and close to a solid surface. For distances $\gtrsim 6 \mu\text{m}$, the experimentally measured flow field is well-approximated by a force dipole model; at smaller distances the dipole model overestimates the flow. Generally, the flow field of *E. coli* differs markedly from those created by higher microorganisms, such as *Chlamydomonas* (37, 38) and *Volvox* (37). With regard to the future classification of flow fields of microorganisms, a decomposition in terms of vector spherical harmonics can provide a useful systematic framework, similar to the classification of the electronic orbital structures in atoms or molecules.

Theories of collective behavior in bacterial suspensions identify as a fundamental process the pairwise interaction of bacteria, often assumed to be dominated by long-range fluid flows established by the action of swimming (25). Our analysis suggests that noise, due to orientational Brownian motion and intrinsic swimming stochasticity, drowns out hydrodynamic effects between two bacteria beyond a surprisingly small length scale of a few microns. This implies that hydrodynamic effects will be relevant only in sufficiently dense bacterial suspensions. However, under such

conditions, the flow structure close to the bacterial body and contact interactions (e.g., flagellar bundling, steric repulsion) will be more important than the asymptotic long-range details of individual microswimmer flow fields.

Insights into the biochemical and physical interactions between bacteria and surfaces are crucial for understanding the dynamics of biofilm formation, the emergence of collective bacterial behavior in boundary layers, and, thus, more generally the evolution from unicellular to multicellular, cooperative forms of life. Our results suggest that long-range hydrodynamic effects play a negligible role in the scattering of *E. coli* with surfaces before collisions. However, hydrodynamic effects can, at least partially, account for the observed trapping of bacteria within a few microns of the surface. The analysis presented herein lends support to the hypothesis (51) that turbulent swarming patterns in bacterial films arise primarily due to steric repulsion and other near-field interactions.

Our experimental and theoretical results favor collision-dominated models (28–30) for the accumulation of bacteria at surfaces over models based on long-range hydrodynamics (27). To obtain a more complete dynamical picture of biofilm formation, future efforts should focus on developing more precise measurement methods and advanced models that include lubrication effects and biochemical bacteria-surface interactions. While our combination of measurements, simulations, and theory shows that long-range physical interactions are negligible for bacterial cell-surface scattering, fluid-mediated coupling could become important for organisms swimming against or in contact with a surface, because the organism is then no longer force-free, resulting in a substantially longer range of hydrodynamic interactions (47, 52).

However, the main implication of the present study is that short-range forces and noise are likely to dominate the interactions between swimming bacteria, so that collective motion in bacterial suspensions, thin films (4, 53), and thin wetting layers (54) relates closely to that seen in driven granular systems (55), assemblages of biofilaments (56), and animal flocks (57, 58). This suggests that many of the principles that determine flocking and self-organization in higher animals should also govern the collective motion of the smallest organisms.

Materials and Methods

A detailed description of the mathematical models is provided in the *SI Text*. The experiments are summarized below.

Culture Conditions. We used *E. coli* strain HCB437 carrying the plasmid pEGFP (Clontech, BD Biosciences), kindly supplied by Douglas B. Weibel (University of Wisconsin-Madison) and Howard C. Berg (Harvard University). Cells were streaked on 1.5% agar plates containing T-broth (1% tryptone, 0.5% NaCl) and 100 $\mu\text{g}/\text{mL}$ ampicillin. A single-colony isolate from an overnight plate was used to inoculate 10 mL of T-broth containing ampicillin and 0.1 mM isopropyl β -D-1-thiogalactopyranoside (IPTG, Sigma), which was then grown for 7 h on a rotary shaker (200 rpm) at 33 °C. This culture was diluted 1:1 with fresh T-broth containing ampicillin and IPTG as above, 0.2% bovine serum albumin, and 0.2 μm fluorescent microspheres (505/515, F8811, Invitrogen) at concentration 9×10^9 beads/mL. This bacterial suspension (approximately 1.6×10^7 cells/mL) was loaded into a polydimethylsiloxane (PDMS) microfluidic device consisting of cylindrical measurement chambers (height 100 μm , radius 750 μm) connected by thin channels. After filling the device, it was sealed to reduce background fluid motion.

Measurement of the Flow Field. Using a Zeiss Axiovert inverted microscope with a 40 \times oil objective (NA 1.3), we simultaneously imaged bacteria and microspheres under fluorescence conditions at 40 fps (Pike, Allied Vision Technologies) and at a temperature of 24 ± 1 °C. To measure the flow field far from walls, we focused on a plane 50 μm inside the chamber to minimize surface effects. To measure the flow field close to a no-slip surface, we focused on a plane 2 μm below the top surface of the sample chamber. Each movie was analyzed with custom Matlab software that precisely tracked bacteria by fitting an ellipsoidal two-dimensional Gaussian shape. For each cell swimming along the focal plane for > 1.5 s, we collected the

instantaneous velocity of all fluorescent tracers up to a distance of 75 μm , using standard particle tracking algorithms. The resulting approximately 5×10^3 tracer velocity vectors were binned into a 0.63 μm square grid (shown in Fig. 1 A and E). The mean of the well-resolved Gaussian distribution in each bin was taken as a local measure of the flow field. To measure the mean residence time of bacteria near a surface, we used the movies that were recorded for measuring the flow field near the wall.

Measurement of the Rotational Diffusion. From the tracks of *E. coli* that swam in the focal plane for >1.5 s, at a distance of 50 μm from the top and bottom surfaces, we determined an average swimming direction at time t by using the direction between the bacterial positions at $t - 0.05$ s and $t + 0.05$ s.

Computing the change in average swimming direction $\Delta\phi$ revealed diffusive scaling, so that we obtained D_r from the equation for two-dimensional orientational diffusion, $\langle(\Delta\phi)^2\rangle = 2D_r\Delta t$, over a time interval Δt . We measured D_r for *Chlamydomonas* with the same procedure, using cell-tracking data described earlier (37).

ACKNOWLEDGMENTS. We are indebted to H. C. Berg and D. B. Weibel for providing bacterial strains and advice, and we thank I. S. Aranson, P. Hänggi, S. Hilbert, T. J. Pedley, P. Talkner, and I. Tuval for discussions, and the reviewers for their comments. This work was supported in part by the Engineering and Physical Sciences Research Council, the Biotechnology and Biological Sciences Research Council, and the European Research Council.

- Pratt LA, Kolter R (1998) Genetic analysis of *Escherichia coli* biofilm formation: Roles of flagella, motility, chemotaxis and type I pili. *Mol Microbiol* 30:285–293.
- Copeland MF, Weibel DB (2009) Bacterial swarming: A model system for studying dynamic self-assembly. *Soft Matter* 5:1174–1187.
- Dombrowski C, et al. (2004) Self-concentration and large-scale coherence in bacterial dynamics. *Phys Rev Lett* 93:098103.
- Wu XL, Libchaber A (2000) Particle diffusion in a quasi-two-dimensional bacterial bath. *Phys Rev Lett* 84:3017–3020.
- Berg HC (2004) *E. coli in Motion* (Springer, New York).
- Stocker R, et al. (2008) Rapid chemotactic response enables marine bacteria to exploit ephemeral microscale nutrient patches. *Proc Natl Acad Sci USA* 105:4209–4214.
- Donlan RM, Costerton JW (2002) Biofilms: Survival mechanisms of clinically relevant microorganisms. *Clin Microbiol Rev* 15:167–193.
- Hall-Stoodley L, Costerton JW, Stoodley P (2004) Bacterial biofilms: From the natural environment to infectious diseases. *Nat Rev Microbiol* 2:95–108.
- Waters CM, Bassler BL (2005) Quorum sensing: Cell-to-cell communication in bacteria. *Annu Rev Cell Dev Biol* 21:319–346.
- Alexander GP, Pooley CM, Yeomans JM (2008) Scattering of low-Reynolds number swimmers. *Phys Rev E Stat Nonlin Soft Matter Phys* 78:045302R.
- Guell DC, Brenner H, Frankel RB, Hartman H (1988) Hydrodynamic forces and band formation in swimming magnetotactic bacteria. *J Theor Biol* 135:525–542.
- Nasseri S, Phan-Thien N (1997) Hydrodynamic interaction between two nearby swimming micromachines. *Comput Mech* 20:551–559.
- Ishikawa T, Sekiya G, Imai Y, Yamaguchi T (2007) Hydrodynamic interactions between two swimming bacteria. *Biophys J* 93:2217–2225.
- Najafi A, Golestanian R (2010) Coherent hydrodynamic coupling for stochastic swimmers. *Europhys Lett* 90:68003.
- Matas Navarro R, Pagonabarraga I (2010) Hydrodynamic interaction between two trapped swimming model micro-organisms. *Eur Phys J E Soft Matter* 33:27–39.
- Gyrya V, Aranson IS, Berlyand LV, Karpeev D (2010) A model of hydrodynamic interaction between swimming bacteria. *Bull Math Biol* 72:148–183.
- Simha RA, Ramaswamy S (2002) Hydrodynamic fluctuations and instabilities in ordered suspensions of self-propelled particles. *Phys Rev Lett* 89:058101.
- Saintillan D, Shelley MJ (2008) Instabilities, pattern formation, and mixing in active suspensions. *Phys Fluids* 20:123304.
- Baskaran A, Marchetti MC (2009) Statistical mechanics and hydrodynamics of bacterial suspensions. *Proc Natl Acad Sci USA* 106:15567–15572.
- Hernandez-Ortiz JP, Stoltz CG, Graham MD (2005) Transport and collective dynamics in suspensions of confined swimming particles. *Phys Rev Lett* 95:204501.
- Haines BM, et al. (2009) Three-dimensional model for the effective viscosity of bacterial suspensions. *Phys Rev E Stat Nonlin Soft Matter Phys* 80:041922.
- Ishikawa T, Locsei JT, Pedley TJ (2008) Development of coherent structures in concentrated suspensions of swimming model micro-organisms. *J Fluid Mech* 615:401–431.
- Putz VB, Dunkel J, Yeomans JM (2010) CUDA simulations of active dumbbell suspensions. *Chem Phys* 375:557–567.
- Batchelor GK (1970) The stress system in a suspension of force-free particles. *J Fluid Mech* 41:545–570.
- Lauga E, Powers TR (2009) The hydrodynamics of swimming microorganisms. *Rep Prog Phys* 72:096601.
- Liao Q, Subramanian G, DeLisa MP, Koch DL, Wu M (2007) Pair velocity correlations among swimming *Escherichia coli* bacteria are determined by force-quadrupole hydrodynamic interactions. *Phys Fluids* 19:061701.
- Berke AP, Turner L, Berg HC, Lauga E (2008) Hydrodynamic attraction of swimming microorganisms by surfaces. *Phys Rev Lett* 101:038102.
- Li G, Tang JX (2009) Accumulation of microswimmers near a surface mediated by collision and rotational Brownian motion. *Phys Rev Lett* 103:078101.
- Elgeti J, Gompper G (2009) Self-propelled rods near surfaces. *Europhys Lett* 85:38002.
- Hernandez-Ortiz JP, Underhill PT, Graham MD (2009) Dynamics of confined suspensions of swimming particles. *J Phys Condens Matter* 21:204107.
- Blake JR, Chwang AT (1974) Fundamental singularities of viscous flow. Part I: The image systems in the vicinity of a stationary no-slip boundary. *J Eng Math* 8:23–29.
- Shum H, Gaffney EA, Smith DJ (2010) Modelling bacterial behaviour close to a no-slip plane boundary: the influence of bacterial geometry. *Proc R Soc Lond A Math Phys Sci* 466:1725–1748.
- Goto T, Nakata K, Baba K, Nishimura M, Magariyam Y (2005) A fluid-dynamic interpretation of the asymmetric motion of singly flagellated bacteria swimming close to a boundary. *Biophys J* 89:3771–3779.
- Smith DJ, Gaffney EA, Blake JR, Kirkman-Brown JC (2009) Human sperm accumulation near surfaces: A simulation study. *J Fluid Mech* 621:289–320.
- Crowdy DG, Or Y (2010) Two-dimensional point singularity model of a low-Reynolds-number swimmer near a wall. *Phys Rev E Stat Nonlin Soft Matter Phys* 81:036313.
- Frymier PD, Ford RM, Berg HC, Cummings PT (1995) Three-dimensional tracking of motile bacteria near a solid planar surface. *Proc Natl Acad Sci USA* 92:6195–6199.
- Drescher K, et al. (2010) Direct measurement of the flow field around swimming microorganisms. *Phys Rev Lett* 105:168101.
- Guasto JS, Johnson KA, Gollub JP (2010) Oscillatory flows induced by microorganisms swimming in two dimensions. *Phys Rev Lett* 105:168102.
- Chattopadhyay S, Moldovan R, Yeung C, Wu XL (2006) Swimming efficiency of bacterium *Escherichia coli*. *Proc Natl Acad Sci USA* 103:13712–13717.
- Darnton NC, Turner L, Rojevsky S, Berg HC (2007) On torque and tumbling in swimming *Escherichia coli*. *J Bacteriol* 189:1756–1764.
- Pepper RE, Roper M, Ryu S, Matsudaira P, Stone HA (2010) Nearby boundaries create eddies near microscopic filter feeders. *J R Soc Interface* 7:851–862.
- Polin M, et al. (2009) *Chlamydomonas* swims with two 'gears' in a eukaryotic version of run-and-tumble locomotion. *Science* 325:487–490.
- Pedley TJ, Kessler JO (1992) Hydrodynamic phenomena in suspensions of swimming microorganisms. *Annu Rev Fluid Mech* 24:313–358.
- Aranson IS, Sokolov A, Kessler JO, Goldstein RE (2007) Model for dynamical coherence in thin films of self-propelled microorganisms. *Phys Rev E Stat Nonlin Soft Matter Phys* 75:040901.
- Ginelli F, Peruani F, Bär M, Chate H (2010) Large-scale collective properties of self-propelled rods. *Phys Rev Lett* 104:184502.
- Subramanian G, Koch DL (2009) Critical bacterial concentration for the onset of collective swimming. *J Fluid Mech* 632:359–400.
- Drescher K, et al. (2009) Dancing *Volvox*: Hydrodynamic bound states of swimming algae. *Phys Rev Lett* 102:168101.
- Böhme U, Scheler U (2007) Effective charge of bovine serum albumin determined by electrophoresis NMR. *Chem Phys Lett* 435:342–345.
- Hänggi P, Talkner P, Borkovec M (1990) Reaction-rate theory: Fifty years after Kramers. *Rev Mod Phys* 62:251–341.
- Dunkel J, Ebeling W, Schimansky-Geier L, Hänggi P (2003) Kramers problem in evolutionary strategies. *Phys Rev E Stat Nonlin Soft Matter Phys* 67:061118.
- Cisneros LH, Kessler JO, Ganguly S, Goldstein RE (2011) Dynamics of swimming bacteria: transition to directional order at high concentration. *Phys Rev E Stat Nonlin Soft Matter Phys* 83:061907.
- Cisneros LH, Kessler JO, Ortiz R, Cortez R, Bees MA (2008) Unexpected bipolar flagellar arrangements and long-range flows driven by bacteria near solid boundaries. *Phys Rev Lett* 101:168102.
- Sokolov A, Aranson IS, Kessler JO, Goldstein RE (2007) Concentration dependence of the collective dynamics of swimming bacteria. *Phys Rev Lett* 98:158102.
- Zhang HP, Be'er A, Florin E-L, Swinney HL (2010) Collective motion and density fluctuations in bacterial colonies. *Proc Natl Acad Sci USA* 107:13626–13630.
- Aranson IS, Tsimring LS (2006) Patterns and collective behavior in granular media: Theoretical concepts. *Rev Mod Phys* 78:641–692.
- Schaller V, et al. (2010) Polar patterns of driven filaments. *Nature* 467:73–77.
- Ramaswamy S (2010) The mechanics and statistics of active matter. *Annu Rev Condens Matter Phys* 1:323–345.
- Buhl J, et al. (2006) From disorder to order in marching locusts. *Science* 312:1402–1406.

Supporting Information

Drescher et al. 10.1073/pnas.1019079108

SI Text

Hydrodynamics vs. Noise in Cell–Cell Scattering. Guided by our experimental results for *Escherichia coli*, we would like to estimate the relative importance of long-range hydrodynamics in cell–cell and cell–surface interactions. To this end, we compare the magnitude of hydrodynamic effects with orientational diffusion due to external noise and intrinsic variability in the bacterial swimming mechanism. To model the hydrodynamic interactions, we use a force dipole approximation to the experimentally determined flow field, as discussed in the main text. Rotational diffusion is quantified by the measured constant $D_r = 0.057 \text{ rad}^2/\text{s}$.

We estimate the mean square change in swimming direction due to hydrodynamic interactions between two bacteria, assuming that the nearest encounter occurs at time $t = 0$ at a distance r . We further assume that a bacterium is approximately ellipsoidal (major axis length a , minor axis length b) and swims at constant speed V_0 . If the unit vector $\mathbf{d}(t)$ denotes the swimming direction of a bacterium at time t , the mean square angular change of the swimming direction during the time interval $[-t/2, t/2]$ is given by

$$\langle \Delta\phi(t, r)^2 \rangle_H := \langle \arccos[\mathbf{d}(-t/2) \cdot \mathbf{d}(t/2)]^2 \rangle_H, \quad [\text{S1}]$$

with $\langle \cdot \rangle_H$ indicating an average over all possible orientations and positions of binary encounters with minimal distance r .

To evaluate the importance of hydrodynamic interactions relative to random fluctuations, we compare $\langle \Delta\phi(t, r)^2 \rangle_H$ with angular diffusion due to Brownian motion and intrinsic swimming variability in three dimensions (3D)

$$\langle \Delta\phi(t)^2 \rangle_D = 4D_r t. \quad [\text{S2}]$$

We can define an effective hydrodynamic radius r_H by means of the condition

$$\langle \Delta\phi(\tau, r_H)^2 \rangle_H = \langle \Delta\phi(\tau)^2 \rangle_D, \quad [\text{S3}]$$

where τ is the characteristic interaction time scale. For scattering events with $r > r_H$ hydrodynamics becomes practically irrelevant. As we shall see below, the final result for r_H will be very robust against changes of the interaction time scale and other parameters.

To obtain an analytical estimate for $\langle \Delta\phi(\tau, r)^2 \rangle_H$, we note that the hydrodynamic change of the unit orientation $\mathbf{d}(t)$ of an ellipsoidal bacterium is given by (1)

$$\dot{\mathbf{d}}_i = \frac{1}{2} \epsilon_{ijk} \omega_j d_k + \Gamma d_k E_{kj} (\delta_{ji} - d_j d_i), \quad [\text{S4}]$$

where the overdot indicates the time-derivative, ϵ_{ijk} is the Levi-Civita tensor, $\omega_i = \epsilon_{ijk} u_{k,j}$ is the vorticity of the fluid field $\mathbf{u}(\mathbf{r})$ at the position of the bacterium, $E_{ij} = (u_{i,j} + u_{j,i})/2$ is the rate-of-strain tensor, and $\Gamma = [(a/b)^2 - 1]/[(a/b)^2 + 1]$ is a geometry factor (we use a summation convention for equal vector and tensor indices, and abbreviate partial derivatives as $u_{i,j} := \partial u_i / \partial r_j$). Our experiments show that the flow field $\mathbf{u}(\mathbf{r})$ generated by a (second) bacterium with unit orientation vector \mathbf{d}' is approximately dipolar,

$$\mathbf{u}_i(\mathbf{r}) = \frac{A}{|\mathbf{r}|^2} [3(\hat{\mathbf{r}} \cdot \mathbf{d}')^2 - 1] \hat{\mathbf{r}}_i, \quad A = \frac{\ell F}{8\pi\eta}, \quad \hat{\mathbf{r}} = \frac{\mathbf{r}}{|\mathbf{r}|}, \quad [\text{S5}]$$

yielding

$$\omega_i = 6A \frac{(\hat{\mathbf{r}} \cdot \mathbf{d}')}{|\mathbf{r}|^3} \epsilon_{ijk} d'_j \hat{\mathbf{r}}_k, \quad [\text{S6}]$$

$$E_{ij} = \frac{A}{|\mathbf{r}|^3} \left\{ [3(\hat{\mathbf{r}} \cdot \mathbf{d}')^2 - 1] \delta_{ij} + 3(\hat{\mathbf{r}} \cdot \mathbf{d}') (d'_j \hat{\mathbf{r}}_i + d'_i \hat{\mathbf{r}}_j) - [15(\hat{\mathbf{r}} \cdot \mathbf{d}')^2 - 3] \hat{\mathbf{r}}_i \hat{\mathbf{r}}_j \right\}. \quad [\text{S7}]$$

Assuming the characteristic scattering time τ is sufficiently small, which is realistic for 3D scattering due to the relatively large swimming speeds of *E. coli*, we can approximate

$$\begin{aligned} \langle \Delta\phi(\tau, r)^2 \rangle_H &\simeq \tau^2 \langle |\dot{\mathbf{d}}(0)|^2 \rangle_H \\ &= 9(\Gamma + 1)^2 \frac{A^2 \tau^2}{r^6} \langle (\hat{\mathbf{r}} \cdot \mathbf{d}')^2 (\mathbf{d} \cdot \mathbf{d}')^2 \rangle_H. \end{aligned}$$

Assuming that $\hat{\mathbf{r}}$ is uniformly distributed on a sphere, and \mathbf{d} uniformly distributed on a circle in the tangential plane at radius r , we obtain

$$\langle \Delta\phi(\tau, r)^2 \rangle_H = \frac{3}{5} (\Gamma + 1)^2 \frac{A^2 \tau^2}{r^6}. \quad [\text{S8}]$$

Equating this expression with rotational diffusion (see Eq. S3) yields the effective hydrodynamic horizon

$$r_H \simeq \left[\frac{3}{20} (\Gamma + 1)^2 \frac{A^2 \tau^2}{D_r} \right]^{1/6}. \quad [\text{S9}]$$

Note that, due to the $\tau^{1/6}$ dependence, the result is rather insensitive to the particular value used for τ and, similarly, to changes in the other parameters. Adopting $\tau = a/V_0$ and inserting experimentally measured values (a, ℓ, F, V, D_r) as given in the main text, we obtain $r_H \simeq 3.3 \mu\text{m}$ for *E. coli*. Eq. S9 can be viewed as an upper bound, as the dipolar flow model overestimates $|\mathbf{u}|$ for $r < 6 \mu\text{m}$ (see Fig. 1D in the main text).

We may thus conclude that (long-range) hydrodynamic interactions will only be of relevance if at least one of the following conditions is satisfied: (i) Bacterial suspensions are sufficiently dense; (ii) self-organization and/or external stimuli lead to orientational and positional correlations between nearby bacteria; (iii) rotational diffusion is strongly suppressed (e.g., through an increase of viscosity). However, our results imply that under natural conditions hydrodynamic long-range interactions are washed out by noise, suggesting that orientational order in dense bacterial suspensions is primarily caused by an interplay of swimming motility and short-range interactions (steric repulsion, lubrication effects, flagellar bundling, etc.) (2).

Hydrodynamic Interactions with a Wall. The previous section focused on the competition between noise and hydrodynamics in bacterial pairwise scattering. We now perform a similar analysis for the hydrodynamic interaction between a bacterium and a wall. Specifically, we are interested in the following two questions (3, 4):

- Is long-range hydrodynamics relevant for bacterial cell–surface scattering?
- Can hydrodynamics trap a bacterium near a wall—and, if so, for how long?

Long-Range Interaction with a Wall. We again approximate the flow field around *E. coli* by a force dipole flow. We denote the position of the dipole by \mathbf{x} , its normalized orientation vector (the bacterial swimming direction) by \mathbf{d} , and the unit normal vector of the solid boundary by \mathbf{n} (pointing into the fluid). Using Blake's solution (5) for a Stokeslet near an infinite planar no-slip surface one can derive explicit expressions for the advective flow $u'_i(\mathbf{x})$, the vorticity $\omega'_k(\mathbf{x})$, and the symmetric rate-of-strain tensor $E'_{ij}(\mathbf{x})$, which act on a force dipole near a wall due to the interaction with its hydrodynamic image (5, 3):

$$u'_j(\mathbf{x}) = \frac{3A}{8h^2} \left\{ 2(\mathbf{n} \cdot \mathbf{d})d_j + [(\mathbf{n} \cdot \mathbf{d})^2 - 1]n_j \right\}, \quad \text{[S10]}$$

$$\omega'_k(\mathbf{x}) = -\frac{3A}{4h^3} (\mathbf{n} \cdot \mathbf{d}) \epsilon_{kin} n_i d_n, \quad \text{[S11]}$$

$$E'_{in}(\mathbf{x}) = \frac{A}{16h^3} \left\{ [5(\mathbf{n} \cdot \mathbf{d})^2 - 1] \delta_{in} - 6d_i d_n - 12(\mathbf{n} \cdot \mathbf{d})(d_i n_n + n_i d_n) + 9[(\mathbf{n} \cdot \mathbf{d})^2 + 1]n_i n_n \right\}, \quad \text{[S12]}$$

where $h := |\mathbf{x} \cdot \mathbf{n}|$ denotes the orthogonal distance to the surface, assuming that the coordinate origin lies on the surface, and ϵ_{ijk} is the Levi-Civita tensor (primes are used to emphasize that the fields in Eqs. S10–S12 contain only the image contribution; for clarity of notation, primes were omitted in the corresponding formulas in main text). Following Pedley and Kessler (1), the deterministic equations of motion for a dipole swimmer that moves at constant swimming speed V_0 in the presence of the wall are given by

$$\dot{\mathbf{x}}_j = V_0 d_j + u'_j(\mathbf{x}), \quad \text{[S13]}$$

$$\dot{d}_j = \frac{1}{2} \epsilon_{jkl} \omega'_k d_l + \Gamma d_i E'_{in} (\delta_{nj} - d_n d_j). \quad \text{[S14]}$$

As before, $\Gamma = [(a/b)^2 - 1]/[(a/b)^2 + 1]$ is a geometric factor for ellipsoidal particles with major axis length a and minor axis length b . The equations S14 for the orientation change can be explicitly written as

$$\dot{d}_j = \frac{3A}{8h^3} (\mathbf{n} \cdot \mathbf{d}) \left\{ 1 - \frac{\Gamma}{2} [3(\mathbf{n} \cdot \mathbf{d})^2 - 1] \right\} [(\mathbf{n} \cdot \mathbf{d})d_j - n_j]. \quad \text{[S15]}$$

To study whether or not long-range hydrodynamics affects the dynamics of a bacterium as it swims towards a wall, we numerically integrated Eqs. S13 and S14 using the experimentally determined parameters for the *E. coli* flow field. The results, which are summarized in Fig. 2 in the main text, show that due to the high swimming speeds of *E. coli*, hydrodynamic long-range interactions are not likely to play an important role in interactions with walls.

Escape from a Wall. An *E. coli*-like (“pusher”) bacterium oriented parallel to a no-slip surface experiences a hydrodynamic attraction towards the surface (3). Orientational noise and swimming may counteract this attraction. We now estimate the typical time it takes for *E. coli* to escape from the wall, using the dipole model defined by Eqs. S10–S15 to see whether such a model can explain the experimentally observed long residence times of bacteria swimming in close proximity to a solid boundary. This model overestimates the effects of hydrodynamics if bacteria come very close to the surface, so that the escape time estimates obtained below should be regarded as approximate upper bounds.

Let us assume that an inelastic collision has led to alignment of the bacterial swimmer parallel to the wall and that, subsequently,

its orientation changes by means of rotational diffusion. We denote by θ the angle between the swimmer and the surface (i.e., $\theta = 0$ means parallel to the surface). The bacterium will be able to escape from the surface, if its swimming velocity component perpendicular to the surface, $V_0(\mathbf{d} \cdot \mathbf{n}) = V_0 \sin \theta$, exceeds the hydrodynamic attraction from the image, $\mathbf{u}' \cdot \mathbf{n}$. Taking the scalar product of Eq. S13 with the wall normal \mathbf{n} , and setting $\dot{\mathbf{x}} \cdot \mathbf{n}$ to zero, defines the escape angle θ_e by

$$\sin \theta_e = \Lambda [1 - 3(\sin \theta_e)^2], \quad \Lambda = \frac{3A}{8h^2 V_0}. \quad \text{[S16]}$$

Solving for θ_e yields

$$\theta_e = \arcsin \left(\frac{-1 + \sqrt{1 + 12\Lambda^2}}{6\Lambda} \right). \quad \text{[S17]}$$

Using the experimental values $A = 31.8 \mu\text{m}^3/\text{s}$ and $V_0 = 22 \mu\text{m}/\text{s}$ for *E. coli*, one finds that $\Lambda < 1$ for distances $h > 0.74 \mu\text{m}$ from the wall; intuitively, the larger the distance from wall the smaller the required escape angle. This suggests that, typically, the escape angle will be small, $\theta_e \ll 1$. In this case, one can approximate

$$\theta_e \simeq \Lambda, \quad \text{[S18]}$$

which becomes quite accurate for *E. coli* parameters when $h > 1.5 \mu\text{m}$. As the dipole model considerably overestimates the actual flow field close to the surface, we can expect that generally $\theta_e \ll 1$.

To estimate the mean escape time, we next consider Eq. S15 for the hydrodynamic torque. Due to the elongated shape of *E. coli*, we can approximate $\Gamma \simeq 1$, and thus find for the component perpendicular to the wall

$$\frac{d}{dt} \sin \theta = -\frac{9A}{16h^3} \sin \theta (\cos \theta)^4. \quad \text{[S19]}$$

This can be rewritten as

$$\dot{\theta} = -\frac{d}{d\theta} U(\theta), \quad \text{[S20]}$$

where the effective angular “potential” $U(\theta)$ is given by

$$U(\theta) = \frac{9A}{64h^3} [1 - (\cos \theta)^4] \quad \text{[S21]}$$

and is normalized such that $U(0) = 0$. During an inelastic collision with the wall, the orientation of the bacterium aligns with the wall, implying that $\theta < \theta_e$. Because θ_e is typically small, as discussed above, one can use the harmonic approximation of the potential in Eq. S21,

$$U(\theta) \simeq \frac{\theta^2}{2\kappa}, \quad \kappa = \frac{16h^3}{9A}, \quad \text{[S22]}$$

where κ defines the characteristic time scale for hydrodynamic realignment in the dipole model.

Eqs. S20 and S21 capture the deterministic torque that acts on the bacterium due to its hydrodynamic image. To account for the stochastic effect of rotational diffusion, we may add a Langevin (6) term to Eq. S20, yielding

$$\dot{\theta} = -\frac{d}{d\theta} U(\theta) + (2D_r^*)^{1/2} \xi(t), \quad \text{[S23]}$$

where D_r^* is the rotational diffusion constant close to the surface in the direction perpendicular to the surface, and $\xi(t)$ denotes

Gaussian white noise characterized by $\langle \xi(t) \rangle = 0$ and $\langle \xi(t)\xi(t') \rangle = \delta(t-t')$. In general, we expect D_r^* to be smaller than the “bare” diffusion constant D_r , measured far from boundaries, due to geometric constraints on the bacterial orientation near a wall.

The Langevin Eq. S23 describes overdamped (angular) Brownian motion in the effective potential $U(\theta)$. Therefore, the question how long a bacterium can be trapped close to a surface reduces to a Kramers problem (6, 7) for the escape over a potential barrier ΔU , which in our case is determined by the escape angle θ_e ,

$$\Delta U = U(\theta_e). \quad \text{[S24]}$$

If the hydrodynamic torque is small, corresponding to a low barrier $\Delta U \ll D_r^*$, the typical time of escape for a bacterium with initial condition $\theta(0) = 0$ is determined by the rotational diffusion time scale

$$t_r(h) \simeq \frac{\theta_e^2}{D_r^*}. \quad \text{[S25]}$$

Using the harmonic approximation (Eq. S22) with $\theta_e \simeq \Lambda$, we may estimate from the condition $\Delta U = D_r^*$ the transition height

$$h_e = \frac{1}{2} \left(\frac{81}{16} \frac{A^3}{D_r^* V_0^2} \right)^{1/7}; \quad \text{[S26]}$$

for $h > h_e$ hydrodynamic effects becomes practically irrelevant. Inserting our experimentally measured values for A , V_0 and the rotational diffusion constant far from surfaces D_r , we find

$$h_e = 1.7 \times \left(\frac{D_r}{D_r^*} \right)^{1/7} \mu\text{m}. \quad \text{[S27]}$$

This means that even for a very small rotational diffusion constant $D_r^* \ll D_r$, the torque exerted by the hydrodynamic image becomes practically negligible if the bacterium is more than a body length away from the surface.

For sufficiently high barriers $\Delta U \gg D_r^*$, standard arguments from transition state theory (6) imply that the mean escape time becomes modified from the rotational diffusion time t_r by an Arrhenius–Kramers factor, so that in this case approximately

$$t_e(h) \approx \left(\frac{\theta_e^2}{D_r^*} \right) \exp\left(\frac{\Delta U}{D_r^*} \right). \quad \text{[S28]}$$

To gain some qualitative insight into the possibility of hydrodynamic trapping close to a surface, we rewrite Eq. S28 in terms of h_e from Eq. S26, adopting as before the harmonic approximation of Eq. S22 with $\theta_e \simeq \Lambda$. This leads to

$$t_e(h) \approx \left(\frac{32}{9} \right) \left(\frac{h_e^7}{A h^4} \right) \exp\left[\left(\frac{h_e}{h} \right)^7 \right], \quad \text{[S29]}$$

which suggests the possibility of a very strong increase of the escape time due to hydrodynamic effects close to the surface.

In practice, Kramers formulas like Eq. S28 often begin to work reasonably well if $\Delta U > 3D_r^*$. Again using the harmonic approximation of Eq. S22 with $\theta_e \simeq \Lambda$, the condition $\Delta U = 3D_r^*$ yields

$$h_K = 1.5 \times \left(\frac{D_r}{D_r^*} \right)^{1/7} \mu\text{m}. \quad \text{[S30]}$$

For *E. coli*, this is approximately the distance where the linear approximation $\theta_e \simeq \Lambda$ becomes valid, so that the right-hand side of Eq. S29 can provide useful qualitative insight into the behavior

of the escape time at distances $h \simeq h_K$, assuming that the dipole model still provides a reasonable approximation in this limit.

Using the quadratic expressions for ΔU with $\theta_e \simeq \Lambda$, and our experimentally measured values for *E. coli* to evaluate the escape time at a distance $h = 1.5 \mu\text{m}$ from the wall, we find

$$t_e \approx 0.78 \times \left(\frac{D_r}{D_r^*} \right) \exp\left[1.99 \times \left(\frac{D_r}{D_r^*} \right) \right] \text{ s}, \quad \text{[S31]}$$

which suggests that bacteria can be temporarily trapped for several seconds, when they come sufficiently close to the surface. Note that, while the distance scales h_e and h_K are very robust to changes in D_r^*/D_r , the mean escape time t_e is very sensitive to variations of this ratio.

In summary, we may conclude that: (i) Hydrodynamics is practically irrelevant if the bacterium is more than a body length away from the surface; (ii) hydrodynamic effects could, at least partially, account for the experimentally observed long escape times of bacteria, when they swim very close ($< 2 \mu\text{m}$) to a solid boundary. However, a more detailed understanding of the long residence times near walls is an important challenge that requires further studies of near-field interactions between bacteria and surfaces.

Spectral Decomposition of Bacterial Flow Fields. An expansion of the flow field $\mathbf{u}(\mathbf{r})$ in terms of vector spherical harmonics yields a systematic decomposition of the angular flow structure. We expect this approach, which is similar to the decomposition of quantum mechanical wave functions in terms of scalar spherical harmonics, to be useful in future studies that aim to classify the fluid flows of different microorganisms, and for comparing experimental data with theoretical models. After summarizing basic definitions, we will demonstrate the method first for dipolar test data and then also for the bacterial flow field measured in our experiments. The notation adopted in this part follows closely that of Hill (8).

Coordinates. It is convenient to consider a three-dimensional (3D) spherical coordinate system

$$r \in [0, \infty), \quad \vartheta \in [0, \pi], \quad \varphi \in [0, 2\pi). \quad \text{[S32]}$$

The radial coordinate r is defined relative to the center of the organism with the Cartesian \hat{z} -axis pointing along the swimming direction. The associated infinitesimal volume element takes the standard form

$$r^2 d\Omega := r^2 \sin \vartheta d\vartheta d\varphi, \quad \text{[S33]}$$

and the locally orthonormal basis vectors of the spherical coordinate system $\{\hat{r}, \hat{\vartheta}, \hat{\varphi}\}$ can be expressed in terms of the Cartesian unit vectors $\{\hat{x}, \hat{y}, \hat{z}\}$ as

$$\hat{r} = \sin \vartheta \cos \varphi \hat{x} + \sin \vartheta \sin \varphi \hat{y} + \cos \vartheta \hat{z}, \quad \text{[S34]}$$

$$\hat{\vartheta} = \cos \vartheta \cos \varphi \hat{x} + \cos \vartheta \sin \varphi \hat{y} - \sin \vartheta \hat{z}, \quad \text{[S35]}$$

$$\hat{\varphi} = -\sin \varphi \hat{x} + \cos \varphi \hat{y}. \quad \text{[S36]}$$

Scalar Spherical Harmonics. The vector spherical harmonics discussed below can be most conveniently expressed in terms of the scalar spherical harmonics

$$Y_{lm}(\vartheta, \varphi) = \left[\frac{2l+1}{4\pi} \frac{(l-m)!}{(l+m)!} \right]^{1/2} P_{lm}(\mu) e^{im\varphi}, \quad \text{[S37]}$$

where $\mu := \cos \vartheta$ and

$$P_{lm}(\mu) = (-1)^m \frac{(1-\mu^2)^{m/2}}{l!2^l} \frac{d^{l+m}}{d\mu^{l+m}} (\mu^2 - 1)^l \quad [\text{S38}]$$

with $l = 0, 1, 2, \dots$, and $m = -l, -l+1, \dots, l$. The scalar spherical harmonics of Eq. S37 satisfy the standard orthonormality relations

$$\int d\Omega Y_{lm} Y_{l'm'}^* = \delta_{ll'} \delta_{mm'}. \quad [\text{S39}]$$

Vector spherical harmonics. Following Hill (8), we define vector spherical harmonics $V_{lm}(\vartheta, \varphi)$, $W_{lm}(\vartheta, \varphi)$, $X_{lm}(\vartheta, \varphi)$ by

$$V_{lm} := \left\{ -\left(\frac{l+1}{2l+1}\right)^{1/2} Y_{lm} \right\} \hat{\mathbf{r}} + \left\{ \frac{1}{[(l+1)(2l+1)]^{1/2}} \frac{\partial Y_{lm}}{\partial \vartheta} \right\} \hat{\boldsymbol{\theta}} + \left\{ \frac{1}{[(l+1)(2l+1)]^{1/2} \sin \vartheta} \frac{\partial Y_{lm}}{\partial \varphi} \right\} \hat{\boldsymbol{\phi}}, \quad [\text{S40}]$$

$$W_{lm} := \left\{ \left(\frac{l}{2l+1}\right)^{1/2} Y_{lm} \right\} \hat{\mathbf{r}} + \left\{ \frac{1}{[l(2l+1)]^{1/2}} \frac{\partial Y_{lm}}{\partial \vartheta} \right\} \hat{\boldsymbol{\theta}} + \left\{ \frac{1}{[l(2l+1)]^{1/2} \sin \vartheta} \frac{\partial Y_{lm}}{\partial \varphi} \right\} \hat{\boldsymbol{\phi}}, \quad [\text{S41}]$$

$$X_{lm} := \left\{ \frac{i}{[l(l+1)]^{1/2} \sin \vartheta} \frac{\partial Y_{lm}}{\partial \varphi} \right\} \hat{\boldsymbol{\theta}} + \left\{ -\frac{i}{[l(l+1)]^{1/2}} \frac{\partial Y_{lm}}{\partial \vartheta} \right\} \hat{\boldsymbol{\phi}}, \quad [\text{S42}]$$

with the additional convention $W_{00} = X_{00} \equiv \mathbf{0}$. For an arbitrary scalar function $f(r)$, we have (8)

$$\nabla \cdot (fV_{lm}) = -\left(\frac{l+1}{2l+1}\right)^{1/2} \left(\frac{df}{dr} + \frac{l+2}{r}f\right) Y_{lm}, \quad [\text{S43}]$$

$$\nabla \cdot (fW_{lm}) = \left(\frac{l}{2l+1}\right)^{1/2} \left(\frac{df}{dr} - \frac{l-1}{r}f\right) Y_{lm}, \quad [\text{S44}]$$

$$\nabla \cdot (fX_{lm}) \equiv 0, \quad [\text{S45}]$$

which implies that the functions X_{lm} are divergence-free

$$\nabla \cdot X_{lm} \equiv 0. \quad [\text{S46}]$$

The vector spherical harmonics from Eqs. S40–S42 fulfill the following orthonormality relations

$$\int d\Omega V_{lm} \cdot V_{l'm'}^* = \delta_{ll'} \delta_{mm'}, \quad [\text{S47}]$$

$$\int d\Omega W_{lm} \cdot W_{l'm'}^* = \delta_{ll'} \delta_{mm'}, \quad [\text{S48}]$$

$$\int d\Omega X_{lm} \cdot X_{l'm'}^* = \delta_{ll'} \delta_{mm'}, \quad [\text{S49}]$$

$$\int d\Omega V_{lm} \cdot W_{l'm'}^* = 0, \quad [\text{S50}]$$

$$\int d\Omega V_{lm} \cdot X_{l'm'}^* = 0, \quad [\text{S51}]$$

$$\int d\Omega W_{lm} \cdot X_{l'm'}^* = 0. \quad [\text{S52}]$$

Hence, an arbitrary vector field $\mathbf{u}(r, \vartheta, \varphi)$ can be decomposed in the form

$$\mathbf{u}(r, \vartheta, \varphi) = \sum_{l=0}^{\infty} \sum_{m=-l}^l u_{lm}^V(r) V_{lm} + \sum_{l=1}^{\infty} \sum_{m=-l}^l u_{lm}^W(r) W_{lm} + \sum_{l=1}^{\infty} \sum_{m=-l}^l u_{lm}^X(r) X_{lm}, \quad [\text{S53}]$$

where the radial coefficient functions $u_{lm}^\gamma(r)$ with $\gamma = V, W, X$ are given by

$$u_{lm}^V(r) := \int d\Omega \mathbf{u}(r, \vartheta, \varphi) \cdot V_{lm}^*(\vartheta, \varphi), \quad [\text{S54}]$$

$$u_{lm}^W(r) := \int d\Omega \mathbf{u}(r, \vartheta, \varphi) \cdot W_{lm}^*(\vartheta, \varphi), \quad [\text{S55}]$$

$$u_{lm}^X(r) := \int d\Omega \mathbf{u}(r, \vartheta, \varphi) \cdot X_{lm}^*(\vartheta, \varphi). \quad [\text{S56}]$$

If the flow field \mathbf{u} is a solution to the incompressible Stokes equations with pressure field p and viscosity η , which means that

$$\eta \nabla^2 \mathbf{u} = \nabla p, \quad \nabla \cdot \mathbf{u} \equiv 0, \quad [\text{S57}]$$

then the coefficient functions $\{u_{lm}^\gamma(r)\}_{\gamma=V,W,X}$ are coupled through Eqs. S57 and the specific boundary conditions that complement these equations.

Extracting Coefficient Functions from 2D Data. Eqs. S53–S56 can be used to systematically decompose 3D flow field data into contributions from different harmonics. In practice, however, the presently available imaging data for bacteria and algae (9) is restricted to the 2D focal plane of the microscope, taken here to be the ($y = 0$)-plane in which the organisms swims. To achieve systematic decomposition in terms of the vector spherical harmonics $\{V_{lm}(\vartheta, \varphi), W_{lm}(\vartheta, \varphi), X_{lm}(\vartheta, \varphi)\}$ in this situation, it is necessary to make additional assumptions about the symmetry of the observed flow fields. For axially symmetric organisms far from boundaries the surrounding average fluid velocity field should be cylindrically symmetric with respect to their body axis $\hat{\mathbf{z}}$, which means that

$$\mathbf{u}(r, \vartheta, \varphi) = R_z(\zeta) \mathbf{u}(r, \vartheta, \varphi + \zeta), \quad \forall (r, \vartheta, \varphi, \zeta), \quad [\text{S58}]$$

where the matrix

$$R_z(\zeta) = \begin{pmatrix} \cos \zeta & -\sin \zeta & 0 \\ \sin \zeta & \cos \zeta & 0 \\ 0 & 0 & 1 \end{pmatrix} \quad [\text{S59}]$$

represents the rotation by an angle ζ about the $\hat{\mathbf{z}}$ -axis. In particular, we have in this case

$$\mathbf{u}(r, \vartheta, \varphi) = R_z(\varphi) \mathbf{u}(r, \vartheta, 0), \quad [\text{S60}]$$

where $\mathbf{u}(r, \vartheta, 0)$ is the field measured in the focal ($y = 0$)-plane. Defining

$$\bar{V}_{lm}(\vartheta) := \int_0^{2\pi} d\varphi R_z(\varphi) V_{lm}, \quad [\text{S61}]$$

$$\bar{W}_{lm}(\vartheta) := \int_0^{2\pi} d\varphi R_z(\varphi) W_{lm}, \quad [\text{S62}]$$

$$\bar{X}_{lm}(\vartheta) := \int_0^{2\pi} d\varphi R_z(\varphi) X_{lm}, \quad [\text{S63}]$$

the expansion coefficients can be written as

$$u_{lm}^V(r) = \int_0^\pi d\vartheta \sin \vartheta \mathbf{u}(r, \vartheta, 0) \cdot \bar{\mathbf{V}}_{lm}^*, \quad [\text{S64}]$$

$$u_{lm}^W(r) = \int_0^\pi d\vartheta \sin \vartheta \mathbf{u}(r, \vartheta, 0) \cdot \bar{\mathbf{W}}_{lm}^*, \quad [\text{S65}]$$

$$u_{lm}^X(r) = \int_0^\pi d\vartheta \sin \vartheta \mathbf{u}(r, \vartheta, 0) \cdot \bar{\mathbf{X}}_{lm}^*. \quad [\text{S66}]$$

Eqs. S64–S66 require knowledge of all three flow components u_x, u_y, u_z , in the ($y = 0$)-plane. In our experiments, we can only measure the flow components in the focal plane, and we therefore set $\mathbf{u}(r, \vartheta, 0) = (u_x, 0, u_z)$, cf. remarks below.

We next illustrate the spectral decomposition of the angular flow field structure for both numerically generated test data and real data from our experiments. To this end, we estimate the integrals in Eqs. S64–S66 numerically using spatially discrete flow field data $\{\mathbf{u}(\mathbf{r}_i)\}$, specified on semicircles of constant radius $|\mathbf{r}_i| = r$, by replacing the integral over ϑ through trapezoidal Riemann sums with the discretization determined by the angular resolution of our data. Generally, the finer the angular resolution $\Delta\vartheta$, the more accurately one can estimate the radial coefficient functions $\{u_{lm}^{\gamma}(r)\}_{\gamma=V,W,X}$. More precisely, we need $N_\vartheta \gg l$, where $N_\vartheta(r)$ is the number of data grid points along the semicircle of radius r . The results presented below are based on a polar grid with angular resolution $\Delta\vartheta = 1^\circ$, corresponding to $N_\vartheta(r) = 181$.

Test Case: Dipolar Flow Field. Our experiments show that the flow $\mathbf{u}(r)$ generated by an *E. coli* bacterium with unit orientation vector \mathbf{d} is well-approximated by a force dipole flow, with components

$$u_i(r) = \frac{A}{|r|^2} [3(\hat{\mathbf{r}} \cdot \mathbf{d})^2 - 1] \hat{r}_i, \quad \hat{\mathbf{r}} = \frac{\mathbf{r}}{|r|}, \quad [\text{S67}]$$

and dipole strength $A \simeq 31.8 \mu\text{m}^3/\text{s}$. To illustrate the flow field decomposition by means of vector spherical harmonics, we first consider test data generated from the ideal force dipole field by computing the components $u_i(r)$ at different radii r on a polar grid with angular spacing $\Delta\vartheta = 1^\circ$. The corresponding flow field for the swimmer orientation $\mathbf{d} = (0, 0, 1)$ is shown in Fig. S1A.

To verify our decomposition procedure, we can insert the coefficient functions $\{u_{lm}^V(r), u_{lm}^W(r), u_{lm}^X(r)\}$, as calculated from Eqs. S64–S66, into the expansion formula (Eq. S53) and compare the resulting flow field with the original velocity field $\mathbf{u}(r)$. The symbols in Fig. S1B and C represent the components of the force dipole flow field at two different radii. The lines indicate the approximation by vector spherical harmonics, obtained with only a finite number of basis functions $\{V_{l'm}(\vartheta, \varphi), W_{l'm}(\vartheta, \varphi), X_{l'm}(\vartheta, \varphi)\}$ with $0 \leq l' \leq l$. As evident from Fig. S1B and C, the quality of the fit to the exact flow data gradually improves the more harmonics one includes. Generally, we find that for $N_\vartheta(r) = 181$ the exact flow field (Eq. S53) is well-approximated when including spherical harmonics with $l' \leq 5$, see Fig. S1B and C.

Experimental Case: Bacterial Flow Field. We now apply an analogous analysis to the experimentally measured flow field, which is shown in Fig. S1D. The corresponding results are summarized in Fig. S1E and F. By comparing the diagrams in Fig. S1E and F with their dipolar counterparts in Fig. S1B and C, one readily observes considerable deviations from the dipolar structure for small distances $r \lesssim 6 \mu\text{m}$, because the anterior-posterior symmetry is broken by the presence of the flagellar bundle. Generally, the decomposition in terms of vector spherical harmonics yields a systematic fitting procedure even at larger distances from the bacterium, when the experimental data becomes noisier, as evident from Fig. S1F.

Angular Kinetic Energy Spectra. The coefficient functions $\{u_{lm}^V(r), u_{lm}^W(r), u_{lm}^X(r)\}$ encode the full radial and angular structure of the bacterial flow field. To obtain a condensed, spectral representation of the flow field structure, we can integrate the local kinetic energy $|\mathbf{u}(r)|^2$ of the flow field over a surface of constant radius r . Using the orthonormality of the vector spherical harmonics, one then finds that the spectral functions

$$p_l(r) := \sum_{m=-l}^l [|u_{lm}^V(r)|^2 + |u_{lm}^W(r)|^2 + |u_{lm}^X(r)|^2] \quad [\text{S68}]$$

measure the average kinetic energy generated by the microorganism at distance r in the angular mode l . The p_l -representation is conceptually similar to the angular power spectrum representation of the cosmic microwave background radiation (10). Fig. 2 shows the p_l -spectra for the dipolar test case and the bacterial flow field at different radii. One readily observes that the front-back asymmetry of the *E. coli* flow field results in an excitation of higher l -modes that are absent for a pure force dipole field. Generally, p_l -spectra can be useful for identifying and quantifying similarities and differences in the flow fields of different types of microorganisms, and for comparing them with theoretical models.

Remarks. The expansion in Eq. S53 provides a useful tool for analyzing the angular structure of flow fields around microorganisms far from boundaries. This opens up the possibility to systematically categorize and compare the flow fields of different bacterial and algal species in terms of their angular vector spectra. While our experimental setup allows us to determine the velocity field only in the 2D focal plane, advanced future experiments might eventually be able to resolve the full 3D flow structure. If this can be achieved, then the additional symmetry assumptions underlying Eqs. S64–S66 can be dropped, and the radial coefficient functions $\{u_{lm}^V(r), u_{lm}^W(r), u_{lm}^X(r)\}$ can be computed directly from Eqs. S54–S56. In principle, one could further decompose the radial coefficient functions in terms of a suitably chosen orthonormal basis system on $[0, \infty)$. The choice of the radial basis functions should be guided by the radial structure of known solutions to the Stokes equations (11).

- Pedley TJ, Kessler JO (1992) Hydrodynamic phenomena in suspensions of swimming microorganisms. *Annu Rev Fluid Mech* 24:313–358.
- Aranson IS, Sokolov A, Kessler JO, Goldstein RE (2007) Model for dynamical coherence in thin films of self-propelled microorganisms. *Phys Rev E Stat Nonlin Soft Matter Phys* 75:040901.
- Berke AP, Turner L, Berg HC, Lauga E (2008) Hydrodynamic attraction of swimming microorganisms by surfaces. *Phys Rev Lett* 101:038102.
- Li G, Tang JX (2009) Accumulation of microswimmers near a surface mediated by collision and rotational brownian motion. *Phys Rev Lett* 103:078101.
- Blake JR, Chwang AT (1974) Fundamental singularities in viscous flow. *J Eng Math* 8:23–29.

- Hänggi P, Talkner P, Borkovec M (1990) Reaction-rate theory: Fifty years after Kramers. *Rev Mod Phys* 62:251–341.
- Dunkel J, Ebeling W, Schimansky-Geier L, Hänggi P (2003) Kramers problem in evolutionary strategies. *Phys Rev* E67:061118
- Hill EL (1954) The theory of vector spherical harmonics. *Amer J Phys* 22:211–214.
- Drescher K, et al. (2010) Direct measurement of the flow field around swimming microorganisms. *Phys Rev Lett* 105:168101.
- Spergel DN, et al. (2007) Three-year Wilkinson microwave anisotropy probe (WMAP) observations: Implications for cosmology. *Astrophys J* 170:377–408.
- Happel J, Brenner H (1983) *Low Reynolds Number Hydrodynamics* (Martinus Nijhoff, The Hague).

